

Quantitative study of electronic whispering gallery modes in electrostatic-potential induced circular graphene junctions

T Lien Le¹ and V Lien Nguyen^{2,3*}

¹*University of Science and Technology of Hanoi, Hanoi, Vietnam*

²*Institute for Bio-Medical Physics, 109A Pasteur, 710115 Hochiminh City, Vietnam*

³*Theoretical and Computational Physics Dept., Institute of Physics, VAST*

10 Dao Tan, Ba Dinh Distr., 118011 Hanoi, Vietnam

(Dated: 15 September 2019)

Abstract

Electronic Whispering Gallery Modes (EWGMs) have been recently observed in several circular graphene junctions, pn and pp' , created in scanning tunnelling microscope experiments. By computing the local density of states within the Dirac-Weyl formalism for massless fermions we demonstrate that the EWGMs may really be emerged in any type of the electrostatic-potential induced circular graphene junctions, including uni-junctions (e.g. np - or pp' -junctions) as well as bipolar-junctions (e.g. pn -heterojunctions). Surprisingly, quantitative analyses show that for all the EWGMs identified (regardless of junction types) the quality (Q) factors seem to be $\leq 10^2$, very small compared to those in ordinary optical whispering gallery modes microresonators, while the corresponding mode radii may tunably be in nanometer-scale. Our theoretical results are in good agreement with existent experimental data, putting a question to the application potential of the EWGMs identified.

I. INTRODUCTION

The optical microresonators (or microcavities) that confine the light to small volumes by resonant recirculation are widely utilised in modern linear and nonlinear optics [1]. The most desirable resonators would confine light without loss and would have resonant frequencies defined precisely. In practice, optical resonators are characterised by the two parameters, the quality factor (Q -factor) and the mode volume (V), that respectively describe the temporal and spatial confinement of light in devices. Resonators with potential applications are those of high Q and small V . It appears that an extremely high value of Q may be achieved in the so-called whispering-gallery microresonators of very small volume [2–5]. In these microresonators, like dielectric microspheres, microdisks, or microtori, the light is effectively confined by repeated total internal reflections at the curved boundaries, giving rise to resonances. The circular optical modes emerged in such resonators are often referred to as Whispering-Gallery Modes (WGMs). The Q -factor of optical WGMs may be as high as $\sim 10^{10}$, depending primarily on the resonator material and a perfection of dielectric surfaces [3]. With a very high Q in combination of other advantages such as very small mode volume and very simple geometry-structure, WGM-resonators emerged as the most potential optical resonators for a variety of applications [2, 3].

As well-known, there is a close similarity between light-rays in geometrical optics and ballistic trajectories of electrons. This similarity attracted much more attention

by the discovery of graphene, in which massless charge-carriers exhibit the photon-like linear dispersion and gain a very large mean-free path (of micrometer even at room temperature) [6]. It was established that the transport of electrons through an electrostatic potential barrier in a graphene heterostructure may well resemble the optical refraction at a surface of metamaterials with negative refractive index [7, 8]. As a consequence, the graphene np -junctions could be perfectly used to create an electronic analogue of Veselago optical lens [7]. And, moreover, the scanning tunnelling microscope (STM)-tip induced circular graphene np -junctions that are extensively exploited to study different properties of Dirac fermions confined by an axially symmetric electrostatic potential barrier [9–11] should act as electronic WGM-resonators in producing circular electronic modes analogous to the optical WGMs. Indeed, recently, electronic Whispering-Gallery Modes (EWGMs) have been reported in several STM-experiments [12–14]. Owing to the dual-gate structure, the back-gate and top-gate, STM-based EWGM-resonators are fully tunable in the meaning that both the resonator size and the np -interface potential may be independently varied by changing suitably the back-gate voltage, the top-gate potential and the tip-to-graphene distance [14]. EWGMs in these resonators can be detected by measuring the tunnelling differential conductance that feature the local density of states (LDOSs) spectrum in dependence on the tip-sample bias, back-gate voltage, and spatial position (from the centre of the tip). So, the observed EWGMs can be theoretically understood by calculating the LDOS for the massless Dirac-like fermions under a suitable tip/gate-induced electrostatic potential. In the continuum calculation reported in Ref. [12] this potential is simply assumed to have the parabolic form,

* nvlien@iop.vast.ac.vn

while in the tight-binding model used in Ref.[14] it is the Thomas-Fermi approximated potential. Both the studies have unambiguously confirmed an emergence of EWGM-spectra in STM-tip induced circular graphene resonators. Here, we note that all the studies in Refs.[12–14] concern the resonators with np/pn -junctions. Very recently, it was reported that similar EWGMs have been observed even in the STM-tip induced circular graphene resonator with pp' -junctions [15].

Actually, EWGMs are known as an almost periodic sequence of resonances emerged in an energy spectrum of a resonator. For the circular graphene resonators under study, these resonances truly describe the quasi-bound states (QBSs) that are formed as a result of interference processes of the electronic waves, undergone multiple Klein-scatterings by the electrostatic confinement potential on the inside of the resonator [16]. Generally, QBSs could be created by any electrostatic confinement potentials [16, 17]. The structure of QBS-spectra however depends on the interference pattern of wave functions inside the resonator, and the later, in turn, is highly sensitive to the characteristics of the confinement potential (such as its magnitudes, signs or sizes). Also, these characteristics are closely correlated with each other in affecting the QBS-spectra. So, it seems that to create a QBS-spectrum with EWGMs in an electrostatic-potential induced circular graphene resonator of any junction-type one has just to set the appropriate characteristics to the confinement potential. And, in principle, EWGMs may emerge in any type of these junctions, though the chance of getting them as well as their quality, i.e. Q -factor and mode volume V , might be different, depending on the junction type. Since these quantities, Q and V , are primary characteristics of EWGMs, one certainly has to determine them first in examining EWGM-spectra.

The purpose of the present theoretical work is to quantitatively study the EWGMs emerged in various models of circular graphene junctions, including uni-junctions such as np -junctions (CGNPJs) or pp' -junctions (CGPP'Js) and bipolar-junctions such as npn -heterojunctions (CGPNPHJs). The junctions are assumed to be created by axially symmetric electrostatic potentials like those in STM-experiments. The study was carried out within the framework the Dirac-Weyl formalism for massless fermions in the presence of the suggested confinement potential. For each of these resonator-models we searched for EWGMs by analysing the LDOSs calculated in wide value-ranges of confinement-potential parameters. For all the identified EWGMs we evaluated the Q -factors and the effective mode radii [18], following the way that is often used for optical WGM-resonators. Qualitatively, our studies demonstrate that the EWGMs may emerge in electrostatic-potential induced circular graphene resonators with any type of junctions, depending primarily on the confinement potential parameters. Quantitative analyses show that for all the EWGMs identified the Q -factors seem always to be $\leq 10^2$, very small compared to those in ordinary optical

WGM-microresonators (of $\simeq 10^5 - 10^8$ [1, 3]), while the corresponding mode radii may tunably be in nanometer-scale. Our theoretical results are in a good agreement with existent experimental data [12, 14, 15], putting a question to the application potential of the EWGM identified.

Thus, we are interested in the circular graphene junctions created by an axially symmetric electrostatic confinement-potential $U(r)$ in a continuous single-layer graphene sheet. Neglecting the valley scattering and using the units such that $\hbar = 1$ and the Fermi velocity $v_F = 1$, the low-energy electronic excitations in these structures can be described by the two-dimensional (2D) massless Dirac-Weyl Hamiltonian:

$$\mathcal{H} = \vec{\sigma}\vec{p} + U(r), \quad (1)$$

where $\vec{\sigma} = (\sigma_x, \sigma_y)$ the Pauli matrices and $\vec{p} = -i(\partial_x, \partial_y)$ the 2D momentum operator. In STM-experiments $U(r)$ is mainly resulted from a combined effect of the tip-sample potential and the back-gate voltage.

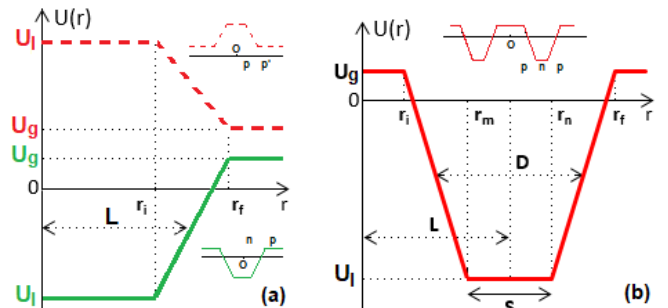


FIG. 1. (color online) Models of radial electrostatic potentials $U(r)$ that create the two types of circular graphene junctions under study: (a) Uni-junctions: green-solid profile - CGNPJs and red-dashed profile - CGPP'Js with average radius L and (b) Bipolar-junctions: red-solid profile - CGPNPHJs with average radius L and average width D . All the modelled potentials are constant at the limiting distances of $r \leq r_i$ and $r \geq r_f$.

Given $U(r)$, we computed LDOSs for the studied resonator, using the approach suggested in Refs.[19, 20](see Supplementary Materials). Shortly, the computing procedure is as following: (i) solving the Dirac equation of Hamiltonian (1) to calculate LDOSs with a given angular momentum j - the partial LDOSs (S4); (ii) taking the sum of partial LDOSs over all possible j provides LDOS $\rho(E, r)$ (S3) that depends on the energy E and the distance r ; and (iii) integrating $\rho(E, r)$ over r provides the total density of states (TDOS) $\rho_T(E)$ (S9). All the features of a resonance spectrum are definitely manifested in its LDOS and TDOS. Certainly, not all junction-samples may reveal EWGMs. So, we had to search for these modes, varying different confinement-potential parameters. Qualitatively, EWGMs can be identified as a spectrum with an almost periodic sequence of resonances, appearing in a narrow range of energy in one side and

close to the charge neutrality point, while in the other side the spectrum shows itself to be featureless [14].

Once a EWGM-spectrum is identified we have quantitatively examined each of most profound resonances in the spectrum by evaluating its partial quality-factor Q_i and partial mode radius R_i [18]. To this end, for the resonance at energy E_i , we measure the resonance width δE_i (by fitting resonance peak into an appropriate Lorentzian profile) and the resonance spacing ΔE_i (see Fig.6(d)). Quantities Q_i and R_i could be then determined in the way as that used for optical WGM-resonators: $Q_i = \omega_i \tau_i \equiv |E_i|/\delta E_i$ and $R_i \approx \hbar v_F/\Delta E_i$, where $\omega_i = |E_i|/\hbar$ is the resonant-mode frequency and $\tau_i = \hbar/2\delta E_i$ is the lifetime of the mode ($\hbar = \text{Planck constant}/2\pi$ and $v_F \approx 10^6 \text{m/s}$ is the Fermi velocity) [3, 4, 12]. From partial quantities [Q_i], [R_i] and [ΔE_i] we respectively deduced the average quantities Q , R and Δ which could be used to characterise the examined EWGM-spectrum on the whole. Such studies have been realised for all the EWGM-spectra identified in circular graphene resonators with different junctions types, uni-junctions CGNPJs and CGPP'Js as well as bipolar-junctions CGPNPHJs.

Thus, first we have to define radial confinement potentials $U(r)$. For the resonators with uni-junctions, the potential $U(r)$ is chosen in the form (see Fig.1(a)):

$$U(r) = \begin{cases} U_l & \text{for } r \leq r_i \\ U_l + \frac{r-r_i}{r_f-r_i}(U_g - U_l) & \text{for } r_i < r < r_f \\ U_g & \text{for } r \geq r_f. \end{cases} \quad (2)$$

The distances r_i and r_f in this equation can be merely expressed as $r_i = (1 - \alpha)L$ and $r_f = (1 + \alpha)L$, where the quantity α with $0 \leq \alpha \leq 1$ and the length L respectively measure the smoothness of the junction-boundary potential and the average radius of the junction (see Fig.1(a)). So, the potential $U(r)$ suggested in eq.(2) is entirely characterised by the four parameters: U_l , U_g , L , and α . In relation to the STM-experiments, the potentials U_g and U_l should be thought of as defined respectively by the back-gate voltage and the tip-sample and back-gate voltages combined, while the two other parameters, L and α , are essentially related to the tip size and the tip-sample distance [14]. The potential $U(r)$ of eq.(2) is quite general, describing all possible circular graphene uni-junctions. Particularly, this potential $U(r)$ describes CGNPJs if $U_l < 0$ and $U_g > 0$. In the other case, when both U_l and U_g are positive, it describes CGPP'Js. Here, it is useful to note that due to the electron-hole symmetry in the models under study a simultaneous change in sign of the two potentials U_l and U_g as well as the energy E does not make the spectrum changed. So, we should consider only two types of uni-junctions, e. g. CGNPJs and CGPP'Js. Certainly, this note should also be applied to the bipolar-junctions introduced below.

In order to model the circular graphene bipolar-junctions, i.e npn - or pnp -heterojunctions, we define the

radial confinement potential $U(r)$ as (see Fig.1(b)).

$$U(r) = \begin{cases} U_g & \text{for } r \leq r_i \\ U_g + \frac{r-r_i}{r_m-r_i}(U_l - U_g) & \text{for } r_i \leq r \leq r_m \\ U_l & \text{for } r_m < r < r_n \\ U_l - \frac{r-r_n}{r_f-r_n}(U_l - U_g) & \text{for } r_n \leq r \leq r_f \\ U_g & \text{for } r \geq r_f. \end{cases} \quad (3)$$

Actually, the labelled distances ($r_\nu, \nu = i, m, n, f$) in this expression can be expressed as $r_i = L - D + S/2$, $r_m = L - S/2$, $r_n = L + S/2$ and $r_f = L + D - S/2$, where L , D , and S may be effectively understood as the average radius of junction, its average width and the tip/top-gate size, respectively (see Fig.1(b)). Thus, in the model suggested a circular graphene bipolar junction is characterised by the five parameters: U_l , U_g , L , D , and S . The potentials U_l and U_g could be here thought of as having the same source as those in the potential of eq.(2). In addition, to describe bipolar-junctions these two potentials must be different in sign, $U_l U_g < 0$, implying the two possible cases of sign-realizations. However, as noted above on the electron-hole symmetry, we need consider only one of these cases, e.g. the case of $U_l < 0$ and $U_g > 0$ (i.e. CGPNPHJs in Fig.1(b)). Note that an equal smoothness is explicitly introduced at both heterojunction boundaries in the potential $U(r)$ of eq.(3).

Importantly, both the potentials in eqs.2 and 3 become constant in the two limits of small and large distances, $r \leq r_i$ and $r \geq r_f$, that would somewhat facilitate the LDOS-computations [20]. In particular case of $U_g \equiv 0$, these potentials $U(r)$ of eqs(2) and (3) seem to have the ordinary trapezoidal profiles. The trapezoidal potentials are often used to describe the gate-induced graphene structures [22, 23], which are also referred to as circular graphene quantum dots [16, 19] or quantum rings [24, 25]. In reality, a trapezoidal shape is quite a good fit of the Lorentzian shape that is widely believed to be the profile of electrostatic potentials induced by a STM-tip [21]. An advantage of the potentials of eqs.(2) and (3) also lies in their simplicity so that the Hamiltonian of eq.(1) could be exactly solved [19, 23].

So, given parameters of the potential $U(r)$ of eq.(2) or eq.(3), as mentioned above, we solved the eigenvalue equation for the Hamiltonian of eq.(1), computed the LDOSs, searched for EWGM-spectra, and quantitatively analysed the EWGMs identified. Searching for EWGMs requires a bit of patience, though some guesses can be made, using experimental data for uni-junctions (for CGNPJs [14] and for CGPP'Js [15]). Anyway, we were able undoubtedly to identify the EWGMs in resonators with any type of junctions under study. In the case of uni-junctions, identified EWGMs resemble well existent experimental data. Below, in Figs.2-3, Fig.4, and Fig.5 we present the computational results for the CGNPJs, CGPP'J, and CGPNPHJ, respectively. These figures have the same structure, showing the qualitative behavior and quantitative characters of the EWGM examined. So, avoiding an unnecessary repeat, most detailed discussions relating to the CGNPJ in Figs.2-3 may also be

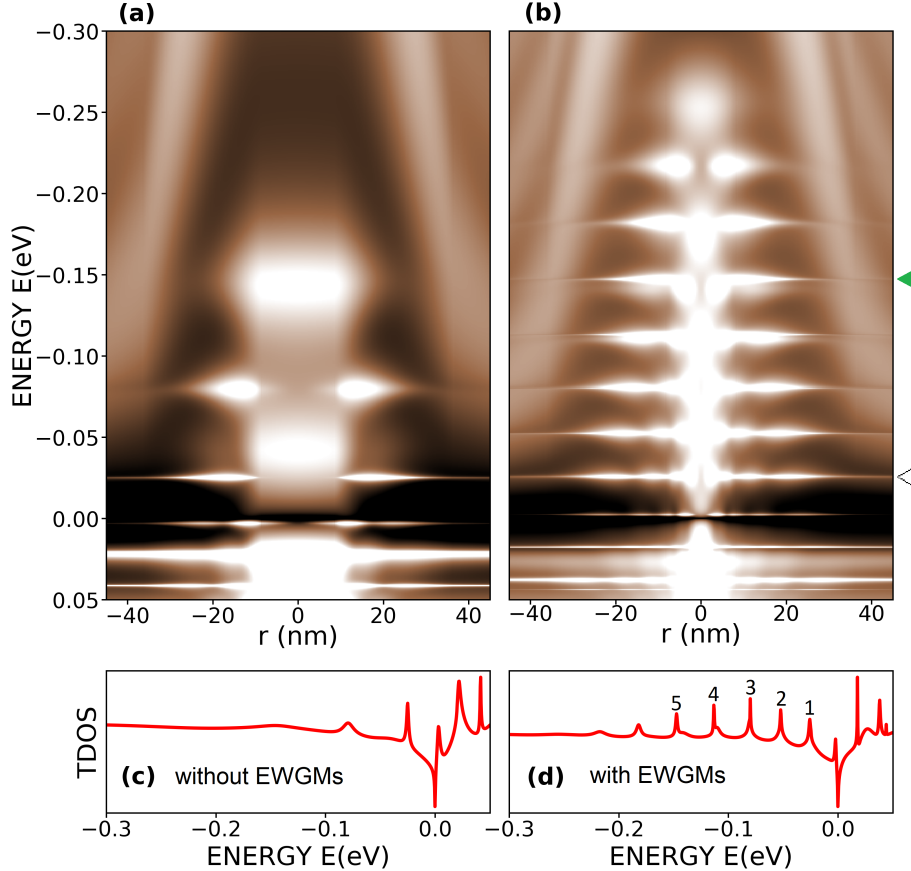


FIG. 2. (color online) (a) Map of LDOS as a function of distance r and (c) corresponding TDOS (in arbitrary unit) for the CGNPJ with potential parameters $[U_i, U_g, L, \alpha] = [-0.35 \text{ eV}, 0.02 \text{ eV}, 15 \text{ nm}, 0.9]$. (b) and (d) are the same as (a) and (c), respectively, but for another CGNPJ with $[U_i, U_g, L, \alpha] = [-0.35 \text{ eV}, 0.02 \text{ eV}, 30 \text{ nm}, 0.5]$. While the spectrum in (a, c) is featureless, that in (b, d) clearly shows EWGMs.

applied to the CGPP'J in Fig.4 as well as the CGPNPHJ in Fig.5.

Fig.2 presents the computed maps of LDOSs as a function of distance r (boxes (a) and (b)) and corresponding TDOSs (boxes (c) and (d)) for the two CGNPJs with different parameter values of the potential of eq.(2) (given in the caption to the figure). Indeed, both the spectra in (c) and (d) show the resonances (or QBSs) which however carry very different features. The spectrum in box (c) is featureless, showing no particular relation between the magnitudes as well as the positions of emerged resonances (Here, one might think of the so-called atomic collapse resonances [26]). On the contrary, the spectrum in box (d) shows an almost periodic sequence of resonances, appeared on one energy-side from the neutral point. This is the typical feature of EWGMs. To ensure that the LDOS in Fig.2(b) really manifests a EWGM-spectrum we should further explore it.

In Fig.3(a) we specifically display the LDOS(E), taken from LDOS(E, r) in Fig.2(b) at different distances r ,

given in the figure. Note that for the CGNPJ-sample studied in this figure the junction-boundary region ranges from $r_i = 15 \text{ nm}$ to $r_f = 45 \text{ nm}$. So, as clearly seen from Fig.3(a), the resonances mainly appear in the boundary region of the junction. In other words, electronic waves are mainly confined at the junction boundary, manifesting a characteristic feature of the EWGM-confinement. A similar conclusion can also be deduced from Fig.3(b), where the spatial distributions of the LDOS are plotted for the two resonances/QBSs marked by the corresponding arrows in Fig.2(b) [27]. The observed ring structure of these distributions is one more manifestation of the EWGM-confinement. Additionally, noting on a difference in the momentum j between these two QBSs, $j = 1/2(7/2)$ for the lower (higher) level in Fig.2(b), we notice that with increasing j the confinement becomes stronger and the electronic wave functions become more localised near the junction boundary. This is in full agreement with the ordinary WGM-idea.

Thus, the TDOS in Fig.2(d) indeed shows itself to be

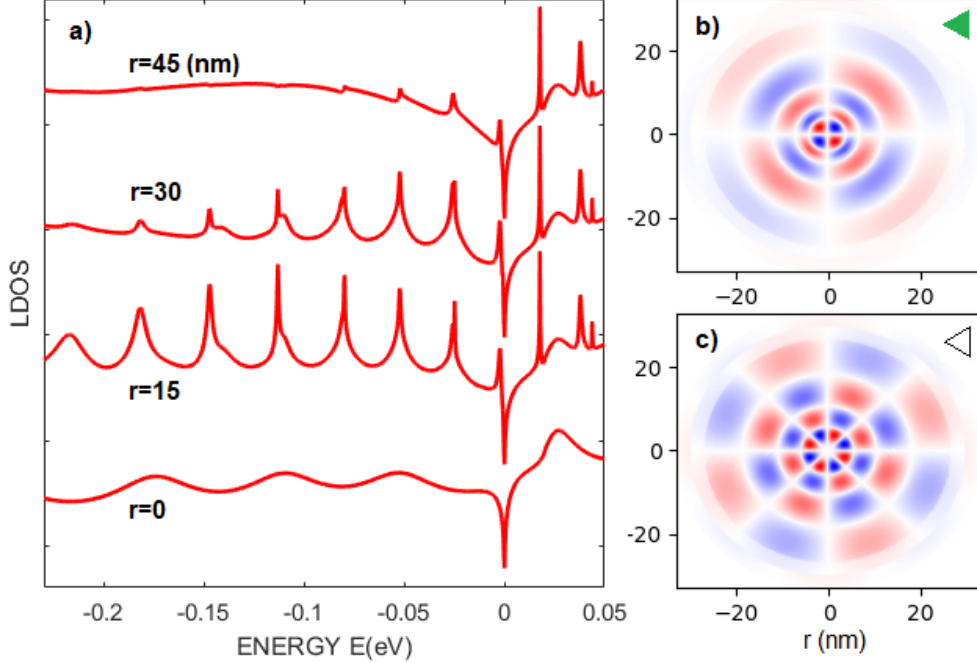


FIG. 3. (color online) (a) LDOSs(E) taken from $LDOS(E, r)$ in Fig.2(b) at different distances r given in the figure; (b) Spatial distributions of the LDOS for the two resonances/QBSs indicated respectively by the arrows in Fig.2(b) [$j = 1/2$ ($7/2$) for the lower (higher) state].

a EWGM-spectrum. To quantitatively evaluate this spectrum we measured the resonance energies E_i , resonance widths δE_i and resonance spacings ΔE_i for the five most profound resonances labelled by the numbers ($i = 1$ to 5) in the spectrum. Then we calculated the partial quality-factors [Q_i] and mode radii [R_i]. Obtained results are as follows: Q_i (eV) \approx 14.23, 34.16, 61.40, 92.34, 78.40 and R_i (nm) \approx 37.56, 36.83, 32.81, 29.73, 29.12 as $i = 1$ to 5. From these data we deduced the average values that characterise the whole EWGM-spectrum in Fig.2(d): the quality factor $Q \approx 47.37$ and the mode radius, $R \approx 31.83$. Also, the resonance spacing ΔE_i seems to slightly increase from 27 meV to 34 meV as i increases from 1 to 5 with the average value of $\Delta \approx 31$ meV. These obtained values of the mode-radius $R \approx 32$ nm and the resonance spacing $\Delta \approx 31$ meV seem to be rather reasonable in relation to the junction size (average radius $L = 30$ nm). Here, as a reference, we would like to mention that the values $R \approx 50$ nm and $\Delta \approx 40$ meV have been reported for the experimental data from Fig.2A in Ref. [12]. Concerning the Q -factor, however, the obtained value $Q \approx 45$ shows a complete surprise, it is too small compared to Q -factors in ordinary optical WGM-microresonators ($\approx 10^5 - 10^8$ [1, 3]). Regretfully, the Q -factor is not claimed in Ref.[12] as well as in the other experiment, relating to the EWGMs in CGNPs [14]. So,

we tried ourselves to get some rough estimations from the data published. Analysing the three most profound resonances labelled 1', 2', and 3' from Fig.2D in Ref.[12] as well as the most profound resonances from Fig.3g in Ref.[14], using the same way as described above, we learn that for all these experimental resonances the partial Q -factors are in the same order of value as the computing Q -factors presented above.

Next, we present in Fig.4 and Fig.5 the computing spectra obtained for a CGPP'J and CGPNPHJ, respectively. It should be again noted that each of Figs.4 and 5 is very similar in both content and structure to Figs.2(b)-(d) plus Fig.3. So, we would like immediately to remark that, like Figs.2-3 for the CGNPJ, Fig.4 (or Fig.5) qualitatively demonstrates an emergence of EWGMs in the CGPP'J (or CGPNPHJ) under study. Note that in accord with the experimental pp' -junction measured in Ref.[15] we have chosen the particular sample with a step junction-boundary potential for the first attempt to study EWGMs in CGPP'Js (in Fig.1(a), step junction-boundary potentials are described by the dashed/solid lines with $x_i \equiv x_f$). And, this is the case reported in Fig.4 (with potential parameters given in the figure).

Quantitatively, analyzing the six most profound resonances labelled by the numbers from 1 to 6 in the TDOS in Fig.4(c), we obtained for the studied

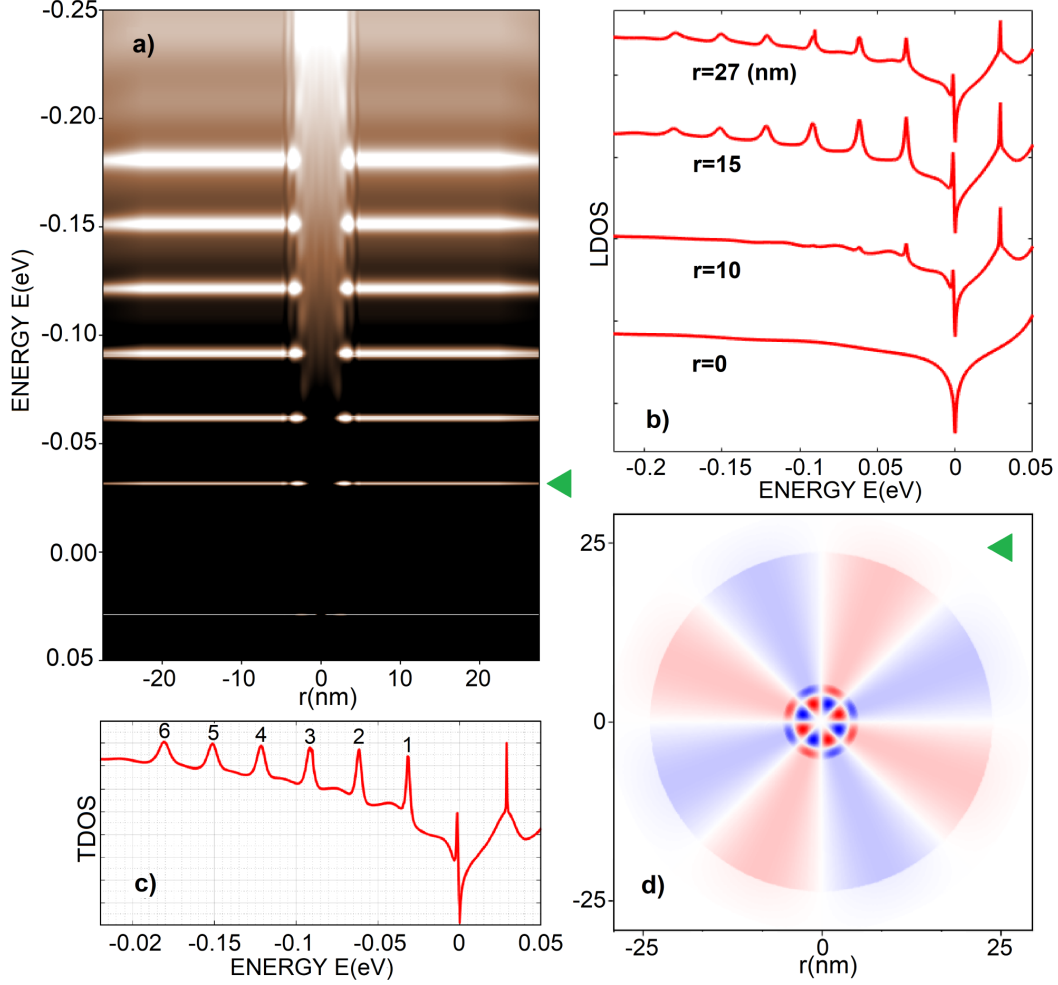


FIG. 4. (color online) (a), (b), (c), and (d) are respectively the same as Fig.2(b), Fig.3(a), Fig.2(d) and Fig.3(b), but for the CGPP'J with potential parameters: $[U_i, U_g, L, \alpha] = [0.28 \text{ eV}, 0.06 \text{ eV}, 25 \text{ nm}, 0.0]$ - step junction-boundary potential.

CGPP'J the partial Q -factors and mode radii as follows: (1) $Q_i \approx 16.09, 45.39, 18.18, 17.49, 16.56$ and 15.74 and (2) $R_i(\text{nm}) \approx 32.49, 33.30, 33.86, 33.58, 33.72$ and 33.86 as $i = 1$ to 6 . So, on the whole, the studied CGPP'J is characterised by the average quality-factor of $Q \approx 21.57$ and mode radius of $R \approx 33.47 \text{ nm}$. Correspondingly, for the resonance spacing that slightly decreases from 31 to 29.7 meV we have the average value $\Delta \approx 30 \text{ meV}$. Analogously, for the six resonances numbered in the TDOS presented in Fig.5(c) we obtained for the studied CGPNPHJ (as $i = 1$ to 6): (1) $Q_i \approx 21.38, 48.53, 40.23, 82.10, 54.64$ and 67.18 with the average value $Q \approx 46.47$; (2) $R_i(\text{nm}) \approx 39.92, 39.64, 38.31, 37.56, 36.36$ and 35.90 with the average mode radius $R \approx 37.51 \text{ nm}$; and (3) The average resonance spacing $\Delta \approx 27 \text{ meV}$. Overall, obtained values of R and Δ are rather reasonable in relation to the potential parameters of the studied junctions. We would here mention that for the CGPP'J measured in the ex-

periment [15] the average level spacing was reported to be 48 meV . Concerning the Q -factors, however, the values obtained for both the CGPP'J in Fig.4 and CGPNPHJ in Fig.5 are very small, in the same order of value as those for CGNPHJs analysed in Figs.2-3 .

Thus, it seems that all the three EWGM-spectra presented in Figs.2-5 for circular graphene resonators of different junction-types show very small values of their Q -factors. A question may then be arisen about if such the small Q -factors are a particular property of the junctions studied. So, we largely searched for EWGMs, varying parameter values of the potential $U(r)$ for each junction type. As a brief summary, we present in Fig.6 the TDOSs with EWGMs for three resonators of each junction type: (a) CGNPHJs; (b) CGPP'Js, and (c) CGPNPHJs (with potential-parameter values given in the figure). Obviously, all these TDOSs show the EWGMs, similar to the TDOSs in Figs.2(a), 4(c) and 5(c). Note that some of these TDOSs are specially collected from the junctions

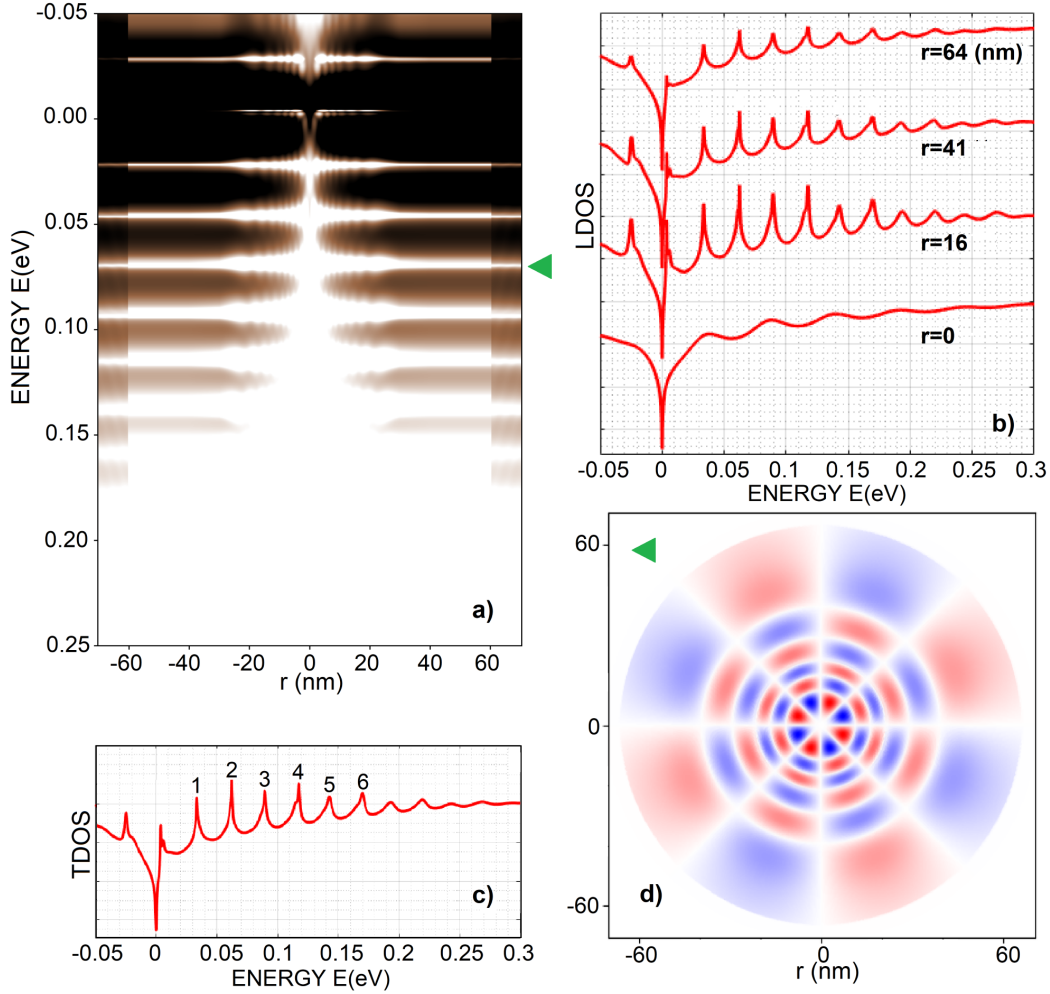


FIG. 5. (color online) (a), (b), (c), and (d) are respectively the same as Fig.2(b), Fig.3(a), Fig.2(d) and Fig.3(b), but for the CGPNPHJ with potential parameters: $[U_l, U_g, L, D, S] = [-0.60 \text{ eV}, 0.15 \text{ eV}, 40 \text{ nm}, 25 \text{ nm}, 2 \text{ nm}]$.

with step junction-boundary potential (in the case of CGPNPHJs, it means $x_i \equiv x_m$ and $x_n \equiv x_f$, see Fig.1(b))

Quantitative analyses of all the EWGM-spectra shown in Fig.6 are in detail given in Tables S1 and S2 (Supplementary Materials). As can be seen in Table S2, the values of mode radii R and resonance spacings Δ obtained for all the examined resonators, (s1) to (s9) (each with five numbered resonances - see Fig.6(a - c)), vary from ≈ 14 to $\approx 67 \text{ nm}$ and from ≈ 15 to $\approx 69 \text{ nm}$, respectively. These values of R and Δ are in the same order of value as the corresponding data reported in Figs.2-5 and seem rather reasonable, depending on the resonator size. As for the quality factors, though the three CGPNPHJs, (s7) to (s9), show somewhat improved values of Q , about a hundred, totally, for all examined resonators, the Q -factors are still small, $\leq 10^2$. We would like here to emphasise that such the Q -factors are found in the EWGMs emerged in all the electrostatic-potential induced circular graphene junctions under study, regardless of the junc-

tion type as well as the smoothness of junction-boundary potentials.

Lastly, we would clarify in Fig.6(c) the way we have used to evaluate the EWGM-characteristics. For the resonance (or QBS) of interest (for instance, the resonance marked by the arrow in the last curve in Fig.6(b)) the quantities to be determined are as follows: (i) the resonance energy E_i that appears as the eigenvalue of the Dirac equation, (ii) the resonance width δE_i that is determined by fitting the resonant peak (dashed line) to an appropriate Lorentzian profile (solid line), following the standard way of evaluating this quantity (see, for example, Ref.[28]), and the resonance spacing ΔE_i that is determined as shown in Fig.6(c). The quantities E_i and δE_i are then used to evaluate partial Q_i and R_i as described above.

In conclusion, we have theoretically studied the EWGMs emerged in energy spectra of electrostatic-potential induced circular graphene junctions, including

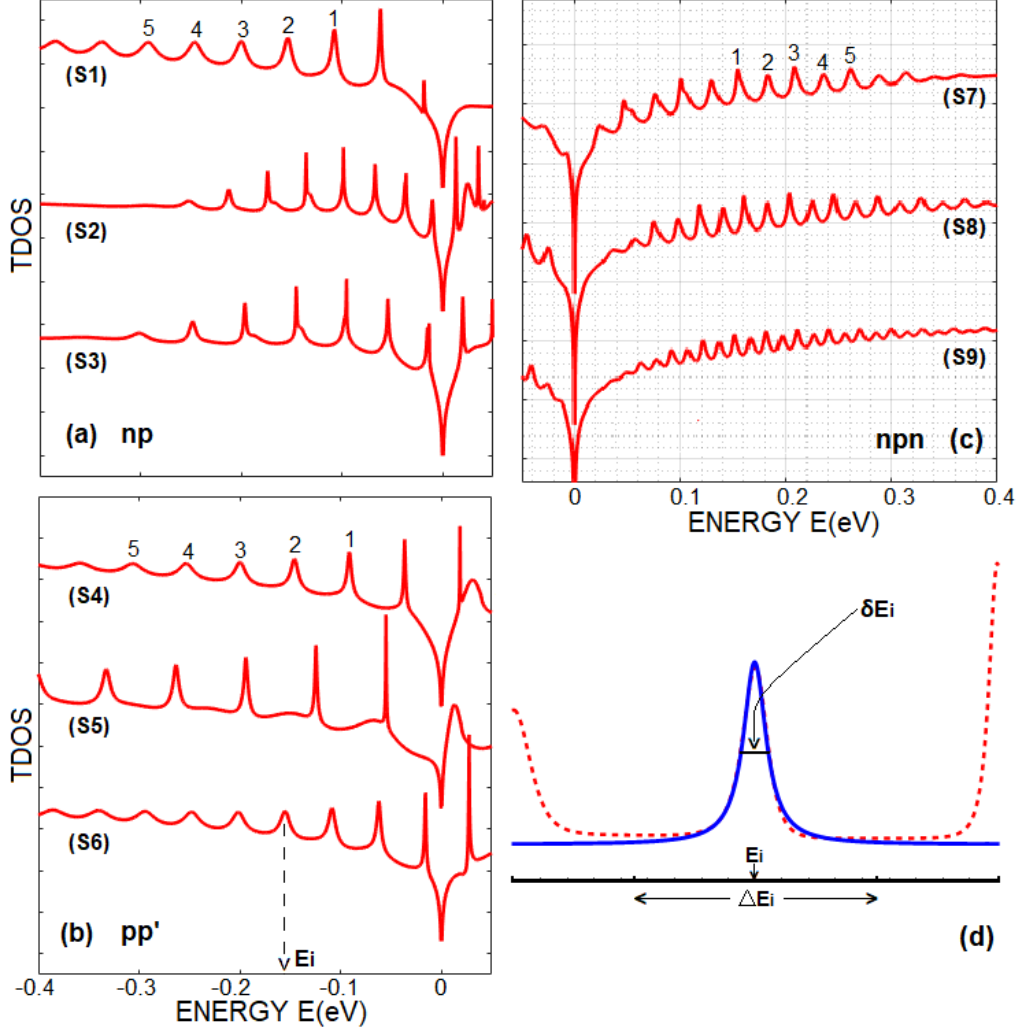


FIG. 6. (color online) The TDOSs are shown for: (a) three CGNPJs with potential parameters $[U_l(\text{eV}), U_g(\text{eV}), L(\text{nm}), \alpha] = [0.15, -0.02, 15, 0.0], [-0.4, 0.02, 27, 0.5]$ and $[-0.5, 0.05, 20, 0.5]$; (b) three CGPP'Js with potential parameters $[U_l(\text{eV}), U_g(\text{eV}), L(\text{nm}), \alpha] = [0.28, 0.04, 13, 0.2], [0.35, 0.02, 10, 0.0]$ and $[0.2, 0.02, 15, 0.1]$; and (c) three CGNP-PHJs with potential parameters $[U_l(\text{eV}), U_g(\text{eV}), L(\text{nm}), D(\text{nm}), S(\text{nm})] = [-0.6, 0.15, 40, 8, 8], [-0.7, 0.3, 50, 15, 2]$ and $[-0.7, 0.3, 70, 15, 2]$. (d) demonstration of the method used to evaluate the partial ΔE_i and δE_i for the resonance at energy E_i (indicated by the arrow from the lowest curve in Fig.6(c): the resonance peak (red-dashed) is fitted to the appropriate Lorentzian profile (solid-blue)

all types of uni-junctions as well as bipolar-junctions. To this end, we modelled the studied junctions by appropriate electrostatic confinement potentials and calculated the LDOSs of structures within the framework of the Dirac-Weyl formalism for massless fermions. Calculations have been carried out for many junction-samples of each junction-type, varying potential-parameter values. From obtained LDOSs we identified those with EWGMs, following the way of identifying the optical WGMs. It seems that EWGMs could be emerged in energy spectra of circular graphene resonators with any junction-type, uni-junctions or bipolar junctions, including those

with a step junction-boundary potential. For all the identified EWGMs we evaluated their characteristics such as the Q -factors, mode radii R , and resonance spacings Δ . Obtained values of R and Δ are rather reasonable, depending on the potential parameters. However, the Q -factors seem always to be surprisingly small (generally, $\leq 10^2$). These theoretical results, including small Q -factors, describe rather well the existent experimental data. We assume that an observed smallness of Q -factors is mainly due to the Klein tunnelling. On the one hand, the Klein tunnelling creates the resonances/QBSs in EWGM-spectra. On the other hand, Klein tunnelling

itself diminishes the resonance/QBS life-times and, therefore, the Q -factors of these resonances. In this view, we would speculate that a smallness of Q -factors is a general property of all graphene resonators created by electrostatic potentials, regardless of resonator shape and size. A magnetic field might enhance a localisation, but it also induces weak resonances, destroying the WGM-feature of

spectra [15].

Acknowledgments. We are very grateful to H.Chau Nguyen for helpful discussions. We also thank T.T. Nhung Nguyen, T.D. Linh Dinh and H. Minh Lam for some collaboration in the first step of numerical computations. This work is funded by Vietnam National Foundation for Science and Technology Development (NAFOSTED) under Grant No. 103.02-2015.48.

-
- [1] Vahala K J 2003 Optical microcavities *Nature* **424** 839
- [2] Oraevsky A N 2002 Whispering-gallery waves *Quantum Electron.* **32** 377
- [3] Matsko A B and V.S. Ilchenko V S 2006 Optical resonators with whispering gallery modes I: Basics *IEEE J.Sel. Top. Quantum Electron.* **12** 3
- [4] Pöllinger M, O'Shea D, Warken F, and Rauschenbeutel A 2009 Ultrahigh- Q Tunable Whispering-Gallery-Mode Microresonator *Phys. Rev. Lett.* **103** 053901
- [5] Acharyya N and Kozyreff G 2019 Large Q -Factor with Very Small Whispering-Gallery-Mode Resonators *Phys. Rev. Appl.* **12** 014060
- [6] Castro Neto A H, Guinea F, Peres N M R, Novoselov K S, and Geim A K 2009 The electronic properties of graphene *Rev. Mod. Phys.* **81** 109
- [7] Cheianov V V, Fal'ko V, and Altshuler B L 2007 The focusing of electron flow and a Veselago lens in graphene p-n junctions *Science* **315** 1252
- [8] Lee G H, Park G H, and Lee H J 2015 Observation of negative refraction of Dirac fermions in graphene *Nature Phys.* **11** 925
- [9] C. Gutierrez C, Brown L, Kim C J, Park J, and Pappathy A N 2016 Klein tunneling and electron trapping in nanometre-scale graphene quantum dots *Nature Phys.* **12** 1069
- [10] Lee J et al. 2016 Imaging electrostatically confined Dirac fermions in graphene quantum dots *Nature Phys.* **12** 1032
- [11] Freitag N M et al. 2016 Electrostatically confined monolayer graphene quantum dots with orbital and valley splittings *Nano Lett.* **16** 5798
- [12] Zhao Y et al. 2015 Creating and probing electron whispering-gallery modes in graphene *Science* **348** 672
- [13] Ghahari F et al. 2017 An on/off Berry phase switch in circular graphene resonators *Science* **356** 845-849
- [14] Jiang Y et al. 2017 Tuning a circular p-n junction in graphene from quantum confinement to optical guiding *Nature Nanotech.* **12** 1045
- [15] Ren Y N et al. 2019 Scanning tunneling microscope characterizations of a circular graphene resonator realized with p - p' junctions *arXiv: 1908.06582 [cond-mat]*
- [16] Matulis A and Peeters F M 2008 Quasibound states in quantum dots in single and bilayer graphene *J. Phys.: Condens. Matter* **77** 115423
- [17] Chen H Y, Apalkov V and Chakraborty T 2007 Fock-Darwin states of Dirac electrons in graphene-based artificial atoms *Phys. Rev. Lett.* **98** 186803.
- [18] There are different definitions of the mode volume for optical WGM-resonators, depending on the problem of interest [2]. Here, instead, we are interested in the mode radius that is entirely definite and may be used to calculate, for instance, the mode area in 2D-resonators [2].
- [19] Nguyen H C, Nguyen N T T, and Nguyen V L 2016 The transfer matrix approach to circular graphene quantum dots *J. Phys.: Condens. Matter* **28** 275301
- [20] Nguyen H C, Nguyen N T T, and Nguyen V L 2017 On the density of states of circular graphene quantum dots *J. Phys.: Condens. Matter* **29** 405301
- [21] Downing C A, Stone D A and Portnoi M E 2011 Zero-energy states in graphene quantum dots and rings *Phys. Rev. B* **84** 155437
- [22] Huard B et al. 2007 Transport measurements across a tunable potential in graphene *Phys. Rev. Lett.* **98** 236803
- [23] Sonin E B 2009 Effect of Klein tunneling on conductance and shot noise in ballistic graphene *Phys. Rev. B* **79** 195438
- [24] Cabosart D, Felten A, Reckinger N, Iordanescu A, Toussaint S, Faniel S, and Hackens B 2017 Recurrent Quantum Scars in a Mesoscopic graphene Ring *Nano Lett.* **17** 1344
- [25] Dinh T D L, Nguyen H C, and Nguyen V L 2018 Quasibound states in single-layer graphene quantum rings *J.Phys.: Condens. Matter* **30** 315501
- [26] Wang Y et al. 2013 Observing Atomic Collapse Resonances in Artificial Nuclei on Graphene *Science* **340** 734
- [27] Fig.3(b), 4(d) and 5(d) have been drawn in the way as that used for similar figures in Ref.[12]: the real part of the second spinor component of the Hamiltonian (1) is plotted for indicated resonances (for spinor components, see Supplementary Materials).
- [28] Davies J H 1998 *The Physics of Low-dimensional semiconductors: an Introduction* (Cambridge: Cambridge University Press)